

PN Acquisition Schemes Using RAKE Structure for DS/SS Systems over a Frequency-Selective Rayleigh Fading Channel

Taweesak Samanchuen¹, Non-member and Sawasd Tantaratana², Member

ABSTRACT

This paper proposes noncoherent PN acquisition schemes that combine the hybrid structure, the RAKE structure, and the double/multiple-dwell technique in order to improve the performance in a frequency-selective fading channel. The hybrid structure reduces the acquisition time compared to a serial scheme. The RAKE structure enhances the received signal strength of a multipath faded signal, while the multiple-dwell technique reduces the acquisition time. The parallel paths of the hybrid structure are used as the RAKE fingers as well, avoiding the need of additional hardware for the RAKE fingers. To further improve the performance, noise-only detection is used in each RAKE finger to nullify the fingers containing only noise in signal combining of the RAKE structure. These helps improve the signal-to-noise ratio at the RAKE output. The performance is evaluated by analysis and simulation. Results show that the proposed schemes significantly outperform other noncoherent PN acquisition schemes with the similar hardware.

Keywords: acquisition, frequency-selective, pseudo-noise, Rayleigh fading, spread spectrum, synchronization

1. INTRODUCTION

Direct-sequence spread-spectrum (DS/SS) technique has been used in many communication systems, due to its advantages, such as interference suppression, energy density reduction, fine time resolution and multiple access capability [1], as well as “soft handoff” in cellular phone systems.

An important component of a SS system is pseudo-noise (PN) which is used for spreading the bandwidth of the message at the transmitter and for despreading the received signal at the receiver. Despreading is possible only if the local PN signal is synchronized with the received PN signal. Therefore, one of the major functions of the receiver is to generate a local PN signal which is synchronous with the incoming

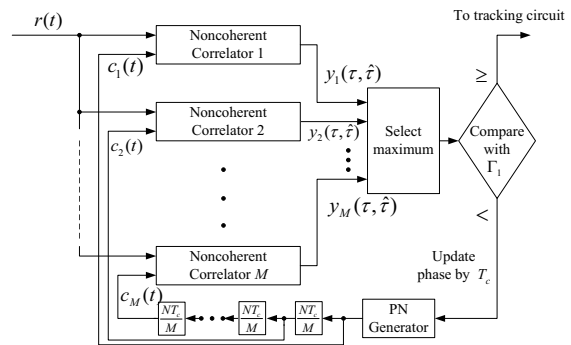


Fig. 1: Conventional hybrid PN acquisition scheme.

PN signal. Traditionally such synchronization is performed in two steps: acquisition (coarse phase alignment) and tracking (fine tuning). There are many techniques of conventional PN acquisition [2, 3]. The simplest technique is the serial search scheme, which searches through all the phases, one at a time, in a serial manner. It uses minimal hardware but the acquisition time is long. On the other hand, the fastest technique is the parallel search scheme, which inspects all the phases simultaneously and picks out the most likely one. However it requires a lot of hardware, which can be prohibitive in some cases. Hybrid schemes of serial and parallel searches provide compromises between acquisition time and hardware. A block diagram of the conventional hybrid scheme is shown in Fig. 1. It consists of M branches of noncoherent correlators, a maximum selector, a threshold test, a PN generator, and a tapped-delay line. In this study this hybrid PN acquisition scheme is used to compare with the proposed scheme.

There are many reports on PN acquisition but most of them assumed a non-fading channel with additive white Gaussian noise (AWGN) [4–6]. If the channel is actually a fading channel, the performances of these schemes would dramatically decrease [7]. To take care of fading, techniques such as using a post-detector or diversity may be employed [8–10].

In cellular systems, the channel may be modeled as a Rician or Rayleigh fading channel. In a Rician fading channel, the received signal consists of a direct path and multiple reflective paths, while the received signal of a Rayleigh fading channel consists of multiple reflective paths without a direct path. The characteristics of fading channels have been explained in

Manuscript received on July 15, 2006 ; revised on October 4, 2006.

^{1,2} The authors are with Sirindhorn International Institute of Technology, Thammasat University, Rangsit Campus, Pathumthani 12121, Thailand. e-mail: sawasd@siit.tu.ac.th

[11], which describes the fading channel in both time and frequency domains. A suitable channel model for DS/SS systems is frequency-selective Rayleigh fading channel because the bandwidth of the DS/SS system is larger than the coherence bandwidth. Frequency-selective fading causes intersymbol interference (ISI), which can be reduced by using a RAKE structure [12]. A RAKE structure exploits the path diversity to increase the signal strength.

In [13], the idea of RAKE structure was applied to acquisition schemes with parallel search, which requires a lot of hardware when the PN length is increased. In [14], the RAKE structure was applied to the serial search scheme. However, it was assumed that the number of multipaths was known to the receiver before the PN acquisition, which is not realistic as the number of multipath is known after PN synchronization (acquisition and tracking). The amount of phase to be updated depends on the number of multipaths hence it was called nonconsecutive search.

In this paper we adapt the RAKE structure for hybrid PN acquisition since it enhances the signal in a multipath environment. The parallel correlators of the hybrid structure are also utilized as the RAKE fingers, so that no additional hardware is required in employing the RAKE technique. In addition, by recognizing that the same hardware can also be used for double-dwell phase alignment test, we apply the double-dwell technique to the RAKE structure to improve the performance without additional hardware. Performance analysis of the RAKE structure with double-dwell test is presented. Further improvement can be obtained by employing multiple-dwell test and employing noise-only detection to exclude the paths without a signal component in the RAKE combining. Results show significant improvement over the conventional hybrid scheme with a similar amount of hardware.

This paper is organized as follows. Section 2 describes the channel model, the proposed scheme and 2 additional modified techniques. Performance of the proposed scheme is analyzed in Section 3. Section 4 presents numerical and simulation results and finally Section 5 concludes this paper.

2. CHANNEL MODEL AND THE PROPOSED SCHEME

2.1 Channel Model

A frequency-selective fading channel for DS/SS can be modeled as a tapped-delay line with a tap spacing of one chip as shown in Fig. 2, where the signal from each tap of the delay line represents a resolvable path of the received signal. The number of resolvable paths is $L_p = \lfloor T_m/T_c \rfloor + 1$ [15], where T_m is the delay spread and T_c is one chip duration. The channel impulse response at time t due to a unit impulse at time ζ is

$$h(t, \zeta) = \sum_{l=0}^{L_p-1} \alpha_l(t) e^{j\theta_l(t)} \delta(t - \zeta - lT_c), \quad (1)$$

where $\alpha_l(t)$ and $\theta_l(t)$ are the gain and phase of the l -th path at time t , respectively. The gains $\alpha_l(t)$, $l = 0, \dots, L_p - 1$, are assumed to be independent and identically distributed (i.i.d.) Rayleigh random variables with a probability density function (pdf) given by

$$f_{\alpha_l}(x) = \frac{2x}{\Omega} \exp\left(-\frac{x^2}{\Omega}\right), \quad x \geq 0 \quad (2)$$

where $E[\alpha_l^2] = \Omega$. For convenience, we normalize Ω to 1. The phases $\theta_l(t)$, $l = 0, \dots, L_p - 1$, are assumed to be i.i.d. random variables uniformly distributed in $[0, 2\pi)$.

The transmitted signal is not only disturbed by the channel characteristics but also by an additive noise, which is assumed to be additive white Gaussian noise (AWGN) with two-sided power spectrum density (PSD) of $N_0/2$ watts per Hertz. The equivalent baseband representation of the received DS/SS signal can be written as

$$r(t) = \sqrt{2P} \sum_{l=0}^{L_p-1} \alpha_l(t) c(t - lT_c - \tau) e^{j\phi_l} + z(t), \quad (3)$$

where P is the average signal power of each path, $c(t)$ is the spreading PN signal, τ is the delay of the first path, $\phi_l = -\omega_c(lT_c + \tau) + \theta_l$, ω_c is the carrier frequency, and $z(t)$ represents the equivalent baseband noise which is a complex white Gaussian noise with two-sided power spectrum density (PSD) of $2N_0$ watts per Hertz [16]. The PN signal $c(t)$ is given by

$$c(t) = \sum_{k=-\infty}^{\infty} c_k P_{T_c}(t - kT_c), \quad (4)$$

where c_k is the k -th chip of the PN sequence and P_{T_c} is the unit-amplitude rectangular pulse in the interval $[0, T_c]$. We wish to obtain an estimate $\hat{\tau}$ of the phase (delay) τ .

A general term to represent the quality of the received signal is the per-chip signal-to-noise ratio (SNR). In the case of a multipath fading channel, SNR should present the average SNR because the power of the received signal fluctuates [17], defined as

$$\text{SNR} = \frac{\bar{P}T_c}{N_0/2} = \frac{2\bar{P}T_c}{N_0}, \quad (5)$$

where \bar{P} is the average received total power. For each resolvable path, we use \bar{P}_l to denote the average received power in the l -th path. Then the average SNR in the l -th path is

$$\text{SNRP}_l = \frac{2\bar{P}_l T_c}{N_0}, \quad (6)$$

where $l = 0, 1, 2, \dots, L_p - 1$. Under the assumption of uniform multipath intensity profile (MIP), all resolvable paths have equal average received power. It follows that SNRP_l are equal for all l , i.e.,

$$\text{SNRP}_l = \text{SNRP} = \frac{\text{SNR}}{L_p} \quad (7)$$

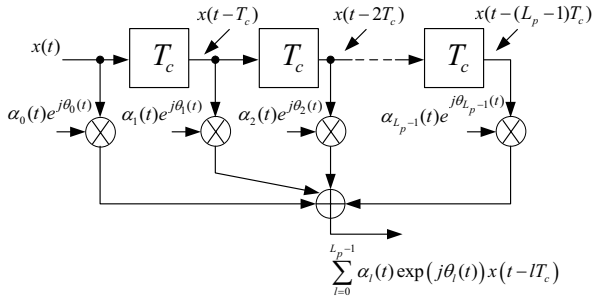


Fig.2: Frequency-selective fading channel model.

and

$$\bar{P}_l = P = \frac{\bar{P}}{L_p}. \quad (8)$$

In the followings, we first describe the proposed hybrid acquisition scheme using RAKE structure and double-dwell test in Subsection 2.2. Then, two modifications for further improvement are presented in Subsections 2.3 and 2.4.

2.2 Proposed Hybrid Scheme using RAKE Structure and Double Dwell Test

The proposed scheme is shown in Fig. 3. It consists of M branches of noncoherent correlators, a decision processing block, a tapped-delay line and a PN generator. The noncoherent detector consists of a multiplier, an integrate-and-dump circuit, real part and imaginary part operators, two square operators and an adder as shown in Fig. 4. There are two integration durations for two operation modes, i.e., $n_1 T_c$ and $n_2 T_c$ for the first step (dwell) and the second step (dwell), respectively. The decision processing block performs four functions, which are summation, threshold test, integrate-and-dump control, and phase update command.

The received signal is fed to the tapped-delay line. The signals tapped from the delay line with spacing of T_c seconds allow the system to capture and combine the signals from the multipaths, as done by a RAKE receiver. After that the signals from the M taps are noncoherently correlated with the local PN signal and the results are sent to the decision processing block. In the first step ($k = 1$), the decision

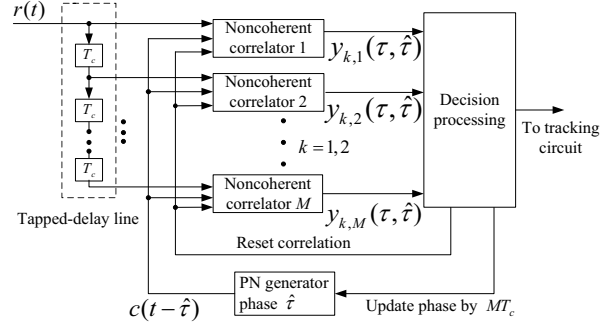


Fig.3: The proposed scheme.

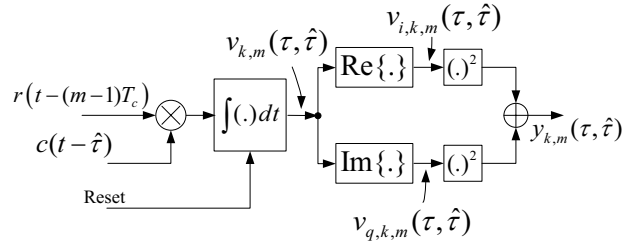


Fig.4: Noncoherent correlator in the m -th branch, $k = 1, 2$.

processing block sums up all the correlated signals together and compares the summation result with a threshold. If it is lower than the threshold, the local PN signal phase, $\hat{\tau}$, is updated by MT_c , the correlators are reset and re-started. On the other hand, if it exceeds the threshold, the process continues in the second step. In the second step ($k = 2$), results of longer correlations are sent to the decision processing block. All of the correlation results are summed together and then compared with the second threshold. If it is lower than the threshold, $\hat{\tau}$ is updated by MT_c and the process goes back to first step. If it exceeds the threshold, the delayed version of the received signal which gives the highest correlation value is sent to the tracking circuit to initiate the fine adjustment process.

The two steps are described in details as follows.

2.2.1 The First Step (First Dwell): Preliminary Detection of Phase Alignment

In the first step, various delayed versions of the received signal $r(t)$ are multiplied with the local PN signal and integrated from 0 to $n_1 T_c$. The value of integration at the m -th branch is

$$v_{1,m}(\tau, \hat{\tau}) = \int_0^{n_1 T_c} \left(\sqrt{2P} \sum_{l=0}^{L_p-1} \alpha_l(t) c(t - lT_c - (m-1)T_c - \tau) e^{j\phi_l} + z(t - (m-1)T_c) \right) c(t - \hat{\tau}) dt, \quad (9)$$

for $m \in \{1, 2, \dots, M\}$, where $z(t)$ is defined in (3). The integration result consists of real and imaginary terms, which are extracted by using real and imaginary extractors. The two resulting signals are squared and summed together. Finally, the output of the m -th noncoherent detector is

$$y_{1,m}(\tau, \hat{\tau}) = v_{i,1,m}^2(\tau, \hat{\tau}) + v_{q,1,m}^2(\tau, \hat{\tau}), \quad (10)$$

where $v_{i,1,m}(\tau, \hat{\tau})$ and $v_{q,1,m}(\tau, \hat{\tau})$ are the real and imaginary parts of $v_{1,m}(\tau, \hat{\tau})$, given by

$$v_{i,1,m}(\tau, \hat{\tau}) = \sum_{l=0}^{L_p-1} \cos(\phi_l) s_{l,1,m}(\tau, \hat{\tau}) + \eta_{i,1,m}, \quad (11)$$

$$v_{q,1,m}(\tau, \hat{\tau}) = \sum_{l=0}^{L_p-1} \sin(\phi_l) s_{l,1,m}(\tau, \hat{\tau}) + \eta_{q,1,m}. \quad (12)$$

The signal $s_{l,1,m}(\tau, \hat{\tau})$ is

$$s_{l,1,m}(\tau, \hat{\tau}) = \sqrt{2P} \int_0^{n_1 T_c} \alpha_l(t) c(t - \hat{\tau}) c(t - lT_c - (m-1)T_c - \tau) dt. \quad (13)$$

The terms $\eta_{i,1,m}$ and $\eta_{q,1,m}$ are the noise parts of $v_{i,1,m}$ and $v_{q,1,m}$, respectively. They are given by

$$\eta_{i,1,m} = \int_0^{n_1 T_c} z_R(t - (m-1)T_c) c(t - \hat{\tau}) dt, \quad (14)$$

$$\eta_{q,1,m} = \int_0^{n_1 T_c} z_I(t - (m-1)T_c) c(t - \hat{\tau}) dt, \quad (15)$$

where $z_R(t)$ and $z_I(t)$ are the real and the imaginary parts of $z(t)$. Each of them is a white Gaussian noise with a two-sided PSD of N_0 watts per Hertz [16]. It can be shown that the noises $\eta_{q,1,m}$ and $\eta_{i,1,m}$ are independent zero mean Gaussian random variables with the same variance of

$$\sigma_{n,1}^2 = n_1 N_0 T_c. \quad (16)$$

Inside the decision processing block, the correlator outputs are summed and compared with the threshold Γ_1 . The summation signal is

$$y_1(\tau, \hat{\tau}) = \sum_{m=1}^M y_{1,m}(\tau, \hat{\tau}). \quad (17)$$

If it exceeds Γ_1 , the correlator goes on to the second step. On the other hand if it is lower than Γ_1 , the phase is updated by MT_c and the correlation is reset.

Note that when the chip timing in a branch is not synchronized, the value of the correlation result is small. Under the situation that there is at least one branch having phase alignment with the local PN signal to within $\pm T_c/2$, the correlation results of those branches will be high. The correlation gives the smallest result under phase alignment when the

phase difference is $T_c/2$, in which case the correlation value is half of the maximum value (since the auto-correlation function has a triangular shape). The signal component of the summation signal $y_1(\tau, \hat{\tau})$ has the smallest value under phase alignment when there is only one branch having phase within $\pm T_c/2$ of the local PN signal and the phase difference is $T_c/2$ or $-T_c/2$. With proper setting of the threshold, the phase alignment can be detected.

2.2.2 The Second Step (Second Dwell) : Verification of Phase Alignment

In the second step, we verify the phase alignment selected by the first step. The value of correlation at the m -th branch is

$$v_{2,m}(\tau, \hat{\tau}) = \int_0^{(n_1+n_2)T_c} \left(\sqrt{2P} \sum_{l=0}^{L_p-1} \alpha_l(t) c(t - lT_c - (m-1)T_c - \tau) e^{j\phi} + z(t - (m-1)T_c) \right) c(t - \hat{\tau}) dt. \quad (18)$$

Similarly to the first step, the integrated signal is separated into the real and imaginary paths. They are squared and summed to obtain the output. The output of the m -th noncoherent correlator is

$$y_{2,m}(\tau, \hat{\tau}) = [v_{i,1,m}(\tau, \hat{\tau}) + v_{i,2,m}(\tau, \hat{\tau})]^2 + [v_{q,1,m}(\tau, \hat{\tau}) + v_{q,2,m}(\tau, \hat{\tau})]^2, \quad (19)$$

where $v_{i,1,m}$ and $v_{q,1,m}$ are the correlation results in the first step, given by (11) and (12), while $v_{i,2,m}$ and $v_{q,2,m}$ are additional correlation results given by

$$v_{i,2,m}(\tau, \hat{\tau}) = \sum_{l=0}^{L_p-1} \cos(\phi_l) s_{l,2,m}(\tau, \hat{\tau}) + \eta_{i,2,m}, \quad (20)$$

$$v_{q,2,m}(\tau, \hat{\tau}) = \sum_{l=0}^{L_p-1} \sin(\phi_l) s_{l,2,m}(\tau, \hat{\tau}) + \eta_{q,2,m}. \quad (21)$$

Here $s_{l,2,m}(\tau, \hat{\tau})$, $\eta_{i,2,m}$ and $\eta_{q,2,m}$ are similar to (13), (14) and (15), respectively, except that the integration duration $(0, n_1 T_c)$ is changed to $(n_1 T_c, (n_1 + n_2) T_c)$. It can be shown that the noises $\eta_{q,2,m}$ and $\eta_{i,2,m}$ are independent zero mean Gaussian random variables with variance $n_2 N_0 T_c$ and the noises $\eta_{i,1,m} + \eta_{i,2,m}$ and $\eta_{q,1,m} + \eta_{q,2,m}$ are also independent zero mean Gaussian random variables with variance

$$\sigma_{n,2}^2 = (n_1 + n_2) N_0 T_c. \quad (22)$$

Similarly to the first step, within the decision processing block, the correlated signals are summed and compared with the threshold Γ_2 . The summation signal is

$$y_2(\tau, \hat{\tau}) = \sum_{m=1}^M y_{2,m}(\tau, \hat{\tau}). \quad (23)$$

If the summation signal is lower than Γ_2 , all the correlators are reset and the process goes back to the first step. On the other hand, if the summation signal is higher than Γ_2 , it has a high probability that one or more of the noncoherent correlators are in-phase with one of the signal paths. We select the phase of the branch with the highest correlation result for tracking. However there is a chance that a wrong phase is selected for tracking (false alarm). The tracking circuit initially sets a time period, during which it tries to track the incoming PN phase. If the time expires and it still cannot track, the tracking is aborted and the process goes back to the first step. This time wasted in an attempt to track the phase due to a false alarm is called “penalty time.”

The length of penalty time depends on the tracking circuit. If the tracking circuit has fast tracking, low jitter and low probability to lose lock, the penalty time is short. However, the penalty time does not depend on the acquisition process. Therefore, most works on PN acquisition treat the penalty time as a parameter, set at some multiple value of the correlation length [3, 8].

2.3 The Proposed Scheme with Noise-Only Detection

The proposed scheme in Subsection 2.2 exploits the advantage of the RAKE structure to its full capability when all fingers of the RAKE structure contain an in-phase PN signal, i.e., each branch has one signal path which is in-phase with the local PN signal. An in-phase signal produces a signal component in addition to noise at the correlator output of a finger, whereas an out-of-phase signal produces only noise at the correlator output of a finger. A finger with signal plus noise enhances the SNR of the combined signal at the RAKE output, whereas a finger with only noise degrades the SNR at the RAKE output.

Therefore, to improve the performance of the proposed scheme, we should exclude noise-only fingers from the RAKE combining. To do so, we use a threshold test to decide whether a finger should or should not be used in the RAKE combining. In each finger, the correlation result is compared to a threshold Γ_f . If the threshold is exceeded, the signal from that finger will be included in the RAKE combining. Otherwise, it is excluded. The use of noise-only detection has been applied to data detection in [18] but we use it for acquisition in this work.

The choice of the threshold Γ_f affects the mean acquisition time (MAT). Simulation is used in determining Γ_f which gives the minimum MAT. However MAT depends on all thresholds, i.e., noise detection threshold and decision thresholds in both the first and second steps. Before picking the value of the noise detection threshold, the decision thresholds of the proposed scheme are found first, using simulation. After that the noise detection threshold is selected from

simulation results.

2.4 The Proposed Scheme with Multiple-Dwell Technique

Another technique to improve the performance of the proposed scheme is to use multiple-dwell test. Note that double-dwell search is a special case of multiple dwell search scheme. It is straightforward to modify the proposed scheme to one using RAKE structure and multiple-dwell technique.

Figure 5 is a typical structure of a K -dwell test, where n_k , $k = 1, \dots, K$, is additional integration length in the k -th dwell. Let y_k be the correlation result after

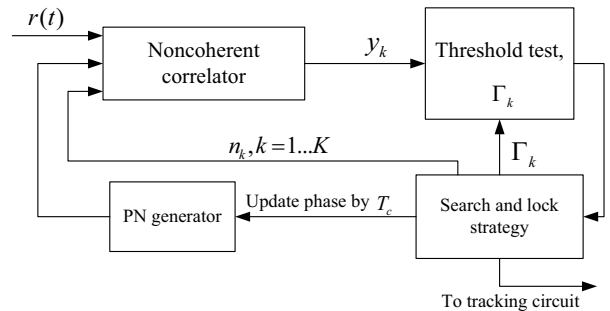


Fig. 5: Multiple-Dwell Test.

the k -th dwell with integration length

$$n^{(k)}T_c = \sum_{i=1}^k n_i T_c. \quad (24)$$

The strategy of immediate rejection is employed for the search. Specifically, if y_k for some $k \in \{1, \dots, K\}$ fails to exceed the threshold Γ_k , then the PN phase will be rejected immediately, whereas phase alignment will be accepted only if y_k exceeds the corresponding threshold Γ_k for all k . This algorithm is applied to the proposed scheme inside the decision processing block in Fig. 3.

One design difficulty of the multiple-dwell technique is how to set the integration lengths, i.e., n_k , and thresholds Γ_k . To simplify this problem, we use the same integration length for all dwells, i.e., $n_1 = n_2 = \dots = n_K$, and then find the thresholds, Γ_k .

Note that the noise-only detection technique in Section 2.3 can be used with the proposed scheme with multiple-dwell test in this section.

2.5 Hardware and Computation Complexity

If we consider the required hardware in the implementation of various schemes, the major portion of the hardware is that of the noncoherent correlators, with some minor portions being those of the PN code generator and delay units. Functions like threshold comparison, accumulation of data, and maximum value selection are implemented by software. Based

on these facts, we can see that the proposed scheme in Fig. 3 has approximately the same hardware as the conventional hybrid scheme in Fig. 1. This is true for all the schemes described in Sections 2.2-2.4 because the noise-only detection and multiple-dwell test are performed by software.

For the computation complexity, the conventional hybrid scheme in Fig. 1 requires a maximum value selection and a threshold comparison. The proposed double-dwell scheme requires a summation of the data from various branches, followed by threshold test, which are repeated if the second dwell is called for. Therefore, in comparison with the conventional scheme, the proposed double-dwell scheme needs the summation operation and one more threshold test. The schemes with noise-only detection and multiple-dwell test need more threshold comparisons and more summation operations. These additional computations are not at all intensive. Therefore, for practical purpose all the proposed schemes require only minor increase in computational complexity.

3. PERFORMANCE ANALYSIS

In this section, performance of the proposed scheme in Subsection 2.2 is analyzed, while the additional techniques in Subsections 2.3 and 2.4 are evaluated by simulation. For PN acquisition, there are several quantities that indicate the performance, e.g., MAT, variance of acquisition time (VAT) and probability density function (pdf) of the acquisition time [19]. In this work MAT and VAT is used for showing the performance.

3.1 Mean Acquisition Time

The PN acquisition can be modeled as a discrete time Markov process. By using the flow graph technique, we can map the state transition diagram of a Markov process to a flow graph and obtain the generating function which contains statistical information. The MAT can be obtained from the derivative of the generating function.

To analyze the performance, we define H_1 as the hypothesis that the local PN phase is within $\pm T_c/2$ of at least one of the PN phases in the incoming L_p paths. Also let H_0 be the hypothesis that the local PN phase is more than $\pm T_c/2$ away from all the PN phases in the incoming L_p paths. Therefore,

$$H_1 : -\frac{T_c}{2} < \xi_l \leq \frac{T_c}{2}, \quad (25)$$

for some $l \in \{1, 2, \dots, L_p\}$,

$$H_0 : (|\xi_1| > \frac{T_c}{2}) \cap (|\xi_2| > \frac{T_c}{2}) \cap \dots \cap (|\xi_{L_p}| > \frac{T_c}{2}), \quad (26)$$

where ξ_l is the phase difference defined by $\xi_l = \hat{\tau} - \tau_l$, with $\tau_l = lT_c + \tau$ being the phase of the l -th path of the received PN signal.

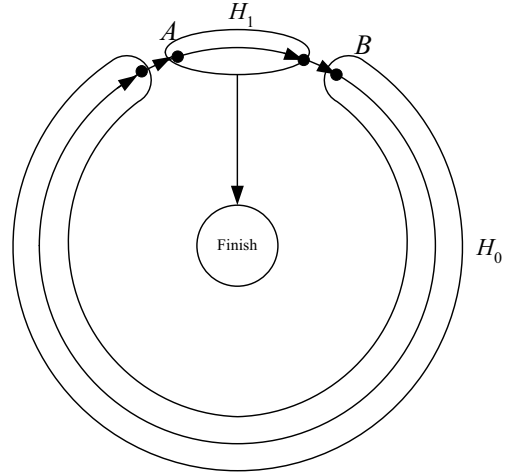


Fig.6: Circular diagram of the proposed scheme.

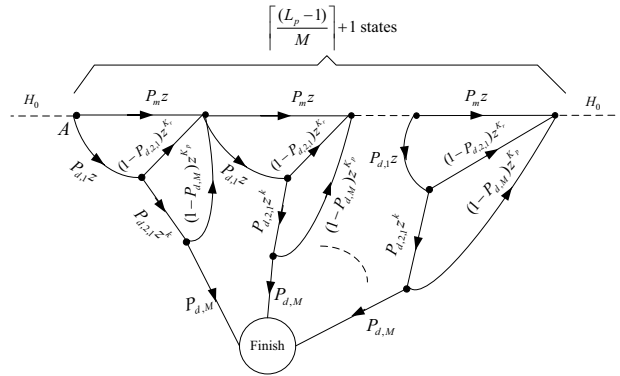


Fig.7: State transition of area H_1 .

The circular state diagram of the proposed scheme can be shown as in Fig. 6. The details inside area H_1 and H_0 are shown in Figs. 7 and 8, respectively, where the parameters are defined as follows.

$$\begin{aligned} P_d &= \Pr \{ (\mathcal{A}) \cap (y_1 \geq \Gamma_1) \cap (y_2 \geq \Gamma_2) | H_1 \}, \\ P_{fa} &= \Pr \{ (y_1 \geq \Gamma_1) \cap (y_2 \geq \Gamma_2) | H_0 \}, \\ P_{d,1} &= \Pr \{ (y_1 \geq \Gamma_1) | H_1 \}, \\ P_{fa,1} &= \Pr \{ (y_1 \geq \Gamma_1) | H_0 \}, \\ P_{d,2} &= \Pr \{ (y_2 \geq \Gamma_2) | (H_1, (y_1 \geq \Gamma_1)) \}, \\ P_{fa,2} &= \Pr \{ (y_2 \geq \Gamma_2) | (H_0, (y_1 \geq \Gamma_1)) \}, \\ P_{d,M} &= \Pr \{ \mathcal{A} | (H_1, (y_1 \geq \Gamma_1), (y_2 \geq \Gamma_2)) \}, \end{aligned} \quad (27)$$

where \mathcal{A} is the event that the branch with the highest correlated signal in the second step is a correct branch, i.e., the difference between local PN phase and the phase of the selected branch is within $\pm T_c/2$.

From the circular diagram and state transition of Figs. 7 and 8, we can draw a simplified flow graph as shown in Fig.9, where

- S is the start state, which can be any of the uncertainty phases,
- F is the finish state,
- A is the first state of area H_1 ,
- B is the first state of area H_0 ,

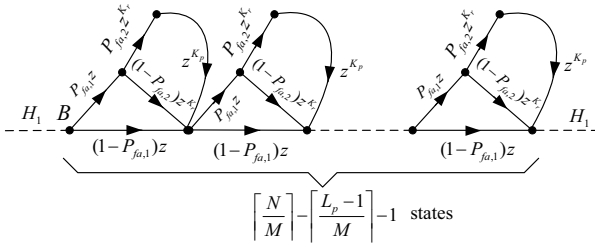


Fig. 8: State transition of area H_0 .

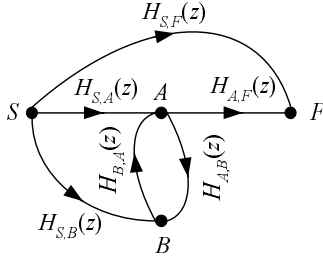


Fig. 9: Simplified flow graph.

- $H_{S,F}(z)$ is transition gain from S to F when the initial phase differences are in H_1 ,
- $H_{S,B}(z)$ is transition gain from S to B when the initial phase differences are in H_1 ,
- $H_{S,A}(z)$ is transition gain from S to A when the initial phase differences are in H_0 ,
- $H_{A,B}(z)$ is transition gain from A to B ,
- $H_{B,A}(z)$ is transition gain from B to A ,
- $H_{A,F}(z)$ is transition gain from A to F .

Expression of the transition gains are

$$H_{B,A}(z) = [P_{fa,1}(1 - P_{fa,2})z^{K_r+1} + P_{fa,1}P_{fa,2}z^{K_p+K_r+1} + (1 - P_{fa,1})z]^{\lfloor \frac{N}{M} \rfloor - \lfloor \frac{L_p-1}{M} \rfloor - 1} \quad (28)$$

$$H_{S,A}(z) = \sum_{n=1}^{\lfloor \frac{N}{M} \rfloor - \lfloor \frac{L_p-1}{M} \rfloor - 1} P_s [P_{fa,1}P_{fa,2}z^{K_p+K_r+1} + P_{fa,1}(1 - P_{fa,2})z^{K_r+1} + (1 - P_{fa,1})z]^n, \quad (29)$$

$$H_{A,B}(z) = [P_{d,1}P_{d,2}(1 - P_{d,M})z^{K_p+K_r+1} + P_{d,1}(1 - P_{d,2})z^{K_r+1} + (1 - P_{d,1})z]^{\lfloor \frac{L_p-1}{M} \rfloor + 1}, \quad (30)$$

$$H_{A,F}(z) = z^{K_r+1}P_{d,1}P_{d,2}P_{d,M} \sum_{i=1}^{\lfloor \frac{L_p-1}{M} \rfloor + 1} [P_{d,1}P_{d,2}(1 - P_{d,M})z^{K_p+K_r+1} + P_{d,1}(1 - P_{d,2})z^{K_r+1} + (1 - P_{d,1})z]^{i-1}, \quad (31)$$

$$H_{S,F}(z) = \sum_{k=0}^{\lfloor \frac{L_p-1}{M} \rfloor} P_s \sum_{i=0}^k [(1 - P_{d,1})z + P_{d,1}P_{d,2}(1 - P_{d,M})z^{K_p+K_r+1} + P_{d,1}(1 - P_{d,2})z^{K_r+1}]^i P_{d,1}P_{d,2}P_{d,M}z^{K_r+1}, \quad (32)$$

$$H_{S,B}(z) = \sum_{i=1}^{\lfloor \frac{L_p-1}{M} \rfloor + 1} [(1 - P_{d,1})z + P_{d,1}P_{d,2}(1 - P_{d,M})z^{K_p+K_r+1} + P_{d,1}(1 - P_{d,2})z^{K_r+1}]^i, \quad (33)$$

where

$$P_s = \left\lfloor \frac{N}{M} \right\rfloor, \quad (34)$$

$$K_r = \frac{n_2}{n_1} \quad (35)$$

and

$$K_p = \frac{\text{Penalty time}}{n_1}. \quad (36)$$

The transfer function $U(z)$ from the Start node to the Finish node obtained from Fig. 9 is

$$U(z) = \frac{H_{A,F}(z)(H_{S,A}(z) + H_{B,A}(z)H_{S,B}(z))}{1 - H_{B,A}(z)H_{A,B}(z) + H_{S,F}(z)}. \quad (37)$$

The first derivative of the transfer function can be used to determine the MAT. Specifically, the MAT is

$$\text{MAT} = \left. \frac{dU(z)}{dz} \right|_{z=1} n_1 T_c. \quad (38)$$

Substituting (37) in (38), we obtain

$$\text{MAT} = nT_c \left(\frac{H'_{A,F}(1)(H_{S,A}(1) + H_{S,B}(1))}{1 - H_M(1)} + \frac{H_{A,F}(1)(H'_{A,B}(1) + H_{A,B}(1)H'_{B,A}(1))}{(H_{A,B}(1) - 1)^2} \cdot \frac{(H_{S,A}(1) + H_{S,B}(1)) + H'_{S,F}(1) + H_{A,F}(1)}{(H'_{S,A}(1) + H'_{B,A}(1)H_{S,B}(1) + H'_{S,B}(1))} \right), \quad (39)$$

where

$$H'_{S,B}(1) = \frac{1}{P_{d,1}^2 P_{d,2}^2 P_{d,M}^2} \left[\left((1 - P_{d,1} P_{d,2} P_{d,M}) \left[\frac{L_p - 1}{M} \right] + 1 \right) \left(\left[\frac{L_p - 1}{M} \right] + 1 \right) P_{d,1} P_{d,2} P_{d,M} + 1 \right) - 1 \right) (-K_r P_{d,1} + K_p P_{d,2} (P_{d,M} - 1) P_{d,1} + (K_r + 1) P_{d,2} P_{d,M} P_{d,1} - 1) \right], \quad (40)$$

$$H_{S,B}(1) = \frac{\left((1 - P_{d,1} P_{d,2} P_{d,M}) \left[\frac{L_p - 1}{M} \right] + 1 - 1 \right)}{P_{d,1} P_{d,2} P_{d,M} (P_{d,1} P_{d,2} P_{d,M} - 1)}, \quad (41)$$

$$H'_{B,A}(1) = \left(\left[\frac{N}{M} \right] - \left[\frac{L_p - 1}{M} \right] - 1 \right) (K_r P_{fa,1} + K_p P_{fa,2} P_{fa,1} + 1), \quad (42)$$

$$H'_{A,B}(1) = (1 - P_{d,1} P_{d,2} P_{d,M}) \left[\frac{L_p - 1}{M} \right] (1 + K_p P_{d,1} P_{d,2} (1 - P_{d,M}) - P_{d,1} P_{d,2} P_{d,M} + K_r P_{d,1} (P_{d,2} - P_{d,M})) \left(\left[\frac{L_p - 1}{M} \right] + 1 \right), \quad (43)$$

$$H_{A,B}(1) = (1 - P_{d,1} P_{d,2} P_{d,M}) \left[\frac{L_p - 1}{M} \right] + 1, \quad (44)$$

$$H'_{S,A}(1) = \sum_{n=1}^{\left[\frac{N}{M} \right] - \left[\frac{L_p - 1}{M} \right] - 1} P_s n (K_r P_{fa,1} + K_p P_{fa,2} P_{fa,1} + 1), \quad (45)$$

$$H_{S,A}(1) = P_s \left(\left[\frac{N}{M} \right] - \left[\frac{L_p - 1}{M} \right] - 1 \right), \quad (46)$$

$$H'_{A,F}(1) = \sum_{i=0}^{\left[\frac{L_p - 1}{M} \right]} P_{d,1} P_{d,2} P_{d,M} (1 - P_{d,1} P_{d,2} P_{d,M})^{i-1} \left((K_r + 1) (1 - P_{d,1} P_{d,2} P_{d,M}) + (1 + K_p P_{d,1} P_{d,2} (1 - P_{d,M}) - P_{d,1} P_{d,2} P_{d,M} + K_r P_{d,1} (1 - P_{d,2} P_{d,M})) \right), \quad (47)$$

$$H_{A,F}(1) = \sum_{i=1}^{\left[\frac{L_p - 1}{M} \right] + 1} P_{d,1} P_{d,2} ((1 - P_{d,2}) P_{d,1} + P_{d,2} (1 - P_{d,M}) P_{d,1} - P_{d,1} + 1)^{i-1} P_{d,M}, \quad (48)$$

$$H'_{S,F}(1) = \sum_{k=0}^{\left[\frac{L_p - 1}{M} \right]} P_s \sum_{i=0}^k i P_{d,1} P_{d,2} P_{d,M} (1 - P_{d,1} P_{d,2} P_{d,M})^{i-1} (K_p P_{d,1} P_{d,2} (1 - P_{d,M}) - P_{d,1} P_{d,2} P_{d,M} + K_r P_{d,1} (1 - P_{d,2} P_{d,M}) + 1), \quad (49)$$

and

$$H_{S,F}(1) = \sum_{k=0}^{\left[\frac{L_p - 1}{M} \right]} P_s \sum_{i=0}^k P_{d,1} P_{d,2} ((1 - P_{d,2}) P_{d,1} + P_{d,2} (1 - P_{d,M}) P_{d,1} - P_{d,1} + 1)^i P_{d,M}. \quad (50)$$

3.2 Probabilities of Detection and False Alarm

Detection probability (P_d) is the probability of accepting phase alignment when H_1 is true, while false alarm probability (P_{fa}) is the probability of accepting phase alignment when H_0 is true. Probabilities of detection and false alarm are important parameters affecting MAT. These two values can be obtained as follow.

Because of the double-dwell technique, P_d and P_{fa} depend on both steps of the detection process. As defined in (27), we can show that

$$P_d = P_{d,1} P_{d,2} P_{d,M}, \quad (51)$$

$$P_{fa} = P_{fa,1} P_{fa,2}. \quad (52)$$

These parameters are controlled by the integration lengths $n_1 T_c$ and $n_2 T_c$, and the thresholds, Γ_1 and Γ_2 .

Probability density functions (pdf) of a noncoherent correlator output $y_{1,m}$ under H_0 and H_1 in the first dwell can be shown to be [9]

$$f_{y_{1,m}}(y|H_0) = \begin{cases} \frac{1}{2\sigma_{1,H_0}^2} \exp\left(-\frac{y}{2\sigma_{1,H_0}^2}\right), & y \geq 0 \\ 0 & \text{otherwise} \end{cases} \quad (53)$$

and

$$f_{y_{1,m}}(y|H_1) = \begin{cases} \frac{1}{2\sigma_{1,H_1}^2} \exp\left(-\frac{y}{2\sigma_{1,H_1}^2}\right), & y \geq 0 \\ 0 & \text{otherwise} \end{cases} \quad (54)$$

respectively. The variances are given by

$$\sigma_{1,H_0}^2 = n_1 PT_c + \sigma_{n,1}^2, \quad (55)$$

$$\sigma_{1,H_1}^2 = PT_c \left(n_1 + 2 \sum_{i=1}^{n_1-1} (n_1 - i) \rho_i \right) + \sigma_{n,1}^2, \quad (56)$$

where ρ_i is the autocorrelation of the fading process given by [17]

$$\rho_i = J_0(2\pi f_d T_c i). \quad (57)$$

Here, J_0 is the zeroth-order Bessel's function and f_d is the maximum Doppler frequency shift.

In the second dwell, the outputs of the noncoherent correlators depend on the values in the first dwell. Therefore the pdf of the output of the noncoherent correlator in the second dwell can be obtained from the conditional pdf's given the value of the first dwell under H_0 and H_1 . The conditional pdf's are [20]

$$f_{y_{2,m}|y_{1,m}}(y_2|y_1, H_0) = \frac{1}{2\sigma_{2,H_0}^2} \exp \left\{ -\frac{y_1 + y_2}{2\sigma_{2,H_0}^2} \right\} I_0 \left(\frac{\sqrt{y_1 y_2}}{\sigma_{2,H_0}^2} \right), \quad y_1, y_2 \geq 0, \quad (58)$$

and

$$f_{y_{2,m}|y_{1,m}}(y_2|y_1, H_1) = \frac{1}{2\sigma_{2,H_1}^2 (1 - \rho^2)} \exp \left\{ \frac{y_2 \sigma_{1,H_1}^2 + y_1 (\sigma_{1,H_1} + \rho \sigma_{2,H_1})^2}{2(\rho^2 - 1) \sigma_{1,H_1}^2 \sigma_{2,H_1}^2} \right\} I_0 \left(\frac{\sqrt{y_1 y_2} (\sigma_{1,H_1} + \rho \sigma_{2,H_1})}{(1 - \rho^2) \sigma_{1,H_1} \sigma_{2,H_1}} \right), \quad y_1, y_2 \geq 0 \quad (59)$$

where

$$\rho = \frac{PT_c}{\sigma_{1,H_1} \sigma_{2,H_1}} \left(\min(n_1, n_2) \sum_{i=\min(n_1, n_2)}^{\max(n_1, n_2)} \rho_i + \sum_{i=\max(n_1, n_2)}^{n_1+n_2-1} (n_1 + n_2 - i) \rho_i + \sum_{i=1}^{\min(n_1, n_2)-1} i \rho_i \right), \quad (60)$$

$$\sigma_{2,H_0}^2 = n_2 PT_c + \sigma_{n,2}^2 \quad (61)$$

and

$$\sigma_{2,H_1}^2 = PT_c \left(n_2 + 2 \sum_{i=1}^{n_2-1} (n_2 - i) \rho_i \right) + \sigma_{n,2}^2. \quad (62)$$

Derivations of the variances σ_{1,H_0}^2 , σ_{2,H_0}^2 , σ_{1,H_1}^2 and σ_{2,H_1}^2 , and correlation coefficient ρ can be found in [7, 20]. Joint pdf's of the outputs in the first and second

dwells are obtained by multiplying (53) and (54) with (58) and (59), respectively, yielding

$$f_{y_{2,m}, y_{1,m}}(y_2, y_1 | H_0) = \frac{1}{4\sigma_{1,H_0}^2 \sigma_{2,H_0}^2} I_0 \left(\frac{\sqrt{y_1 y_2}}{\sigma_{2,H_0}^2} \right) \exp \left\{ -\frac{y_1}{2\sigma_{1,H_0}^2} - \frac{y_1 + y_2}{2\sigma_{2,H_0}^2} \right\}, \quad y_1, y_2 \geq 0, \quad (63)$$

and

$$f_{y_{2,m}, y_{1,m}}(y_2, y_1 | H_1) = \frac{1}{4\sigma_{1,H_1}^2 \sigma_{2,H_1}^2 (1 - \rho^2)} I_0 \left(\frac{\sqrt{y_1 y_2} \left(\frac{\rho \sigma_{2,H_1}}{\sigma_{1,H_1}} + 1 \right)}{(1 - \rho^2) \sigma_{2,H_1}^2} \right) \exp \left\{ \frac{\left(y_1 \left(\frac{\rho \sigma_{2,H_1}}{\sigma_{1,H_1}} + 1 \right)^2 + y_2 \right)}{2(\rho^2 - 1) \sigma_{2,H_1}^2} - \frac{y_1}{2\sigma_{1,H_1}^2} \right\}, \quad y_1, y_2 \geq 0. \quad (64)$$

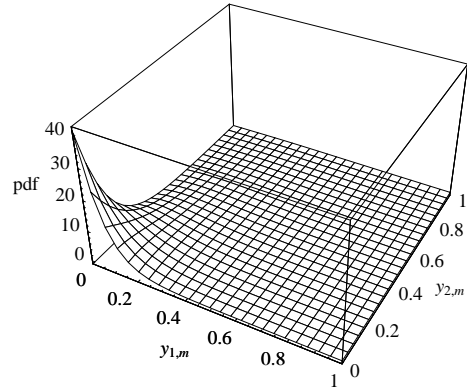


Fig.10: Joint pdf of $y_{1,m}$ and $y_{2,m}$ given H_0 .

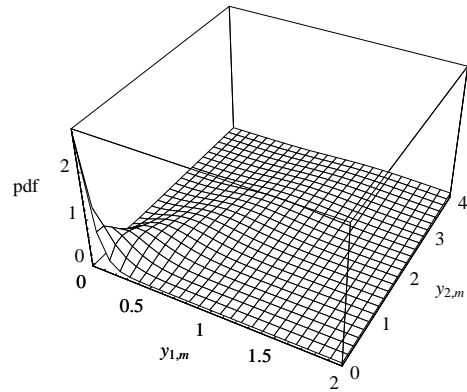


Fig.11: Joint pdf of $y_{1,m}$ and $y_{2,m}$ given H_1 .

Figures 10 and 11 show examples of (63) and (64), which are normalized by σ_{1,H_1}^2 , where $n_1 = 40$,

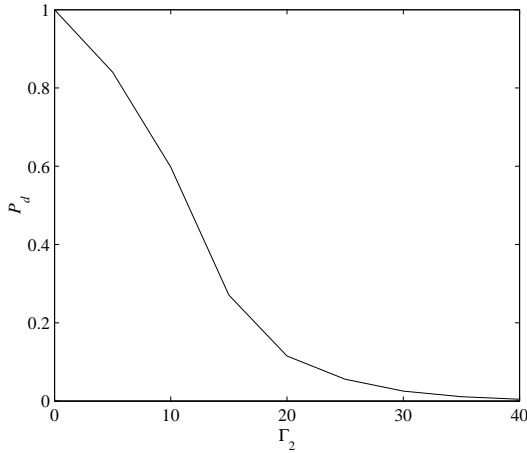


Fig.12: Detection probability by varying threshold in second dwell (Γ_2).

$n_2 = 60$, SNR = -5 dB and $f_d = 10$ Hz. Figure 10 is the joint pdf of $y_{1,m}$ and $y_{2,m}$ given H_0 , from which we can see that most of the mass is concentrated around the origin. The joint pdf $y_{1,m}$ and $y_{2,m}$ given H_1 is shown in Fig. 11, which shows distribution of the mass away from the origin, as compared to the joint pdf given H_0 . This is because of the signal component.

For detecting the in-phase condition, $y_{1,m}$ or $y_{2,m}$, $m = 1, \dots, M$, are summed together and compared with the threshold. One way to find P_d and P_{fa} is to evaluate the pdf of the summation signal, which is difficult to obtain because of the multiple variables and the dependence of the first and second dwells. Alternatively, we can compute the probability of detection by using the joint pdf of all branches and find the integration over the appropriate area.

Because all paths of the received signal are independent, it follows that the outputs of all branches are independent. Therefore, the joint pdf of all branches is

$$f_{y_{1,1}, \dots, y_{1,M}, y_{2,1}, \dots, y_{2,M}}(y_{1,1}, \dots, y_{1,M}, y_{2,1}, \dots, y_{2,M}) = \prod_{m=1}^M f_{y_{1,m}, y_{2,m}}(y_{1,m}, y_{2,m}). \quad (65)$$

Then, the detection probability is

$$P_d = \int \dots \int_{\{\sum_{m=1}^M y_{2,m} \geq \Gamma_2, \sum_{m=1}^M y_{1,m} \geq \Gamma_1\}} \int \dots \int \prod_{m=1}^M f_{y_{1,m}, y_{2,m}}(y_{1,m}, y_{2,m} | H_1) dy_{1,1} \dots dy_{1,M} dy_{2,1} \dots dy_{2,M} \quad (66)$$

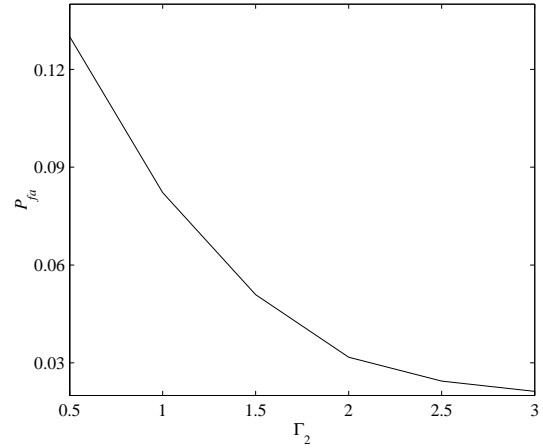


Fig.13: False alarm probability by varying threshold in second dwell (Γ_2).

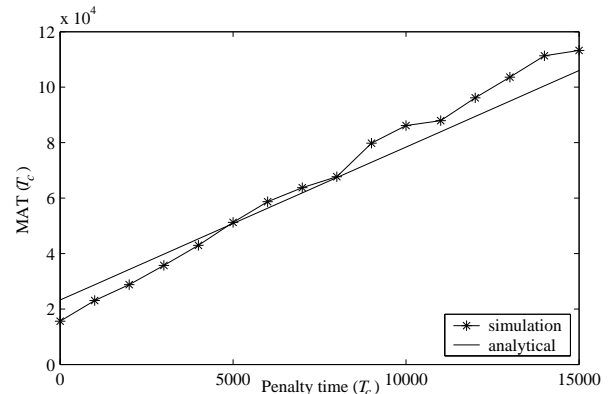


Fig.14: Simulation and analytical result of the proposed scheme.

and the false alarm probability is

$$P_{fa} = \int \dots \int_{\{\sum_{m=1}^M y_{2,m} \geq \Gamma_2, \sum_{m=1}^M y_{1,m} \geq \Gamma_1\}} \prod_{m=1}^M f_{y_{1,m}, y_{2,m}}(y_{1,m}, y_{2,m} | H_0) dy_{1,1} \dots dy_{1,M} dy_{2,1} \dots dy_{2,M}. \quad (67)$$

Note that evaluations of (66) and (67) can be done numerically, but they are computationally intensive.

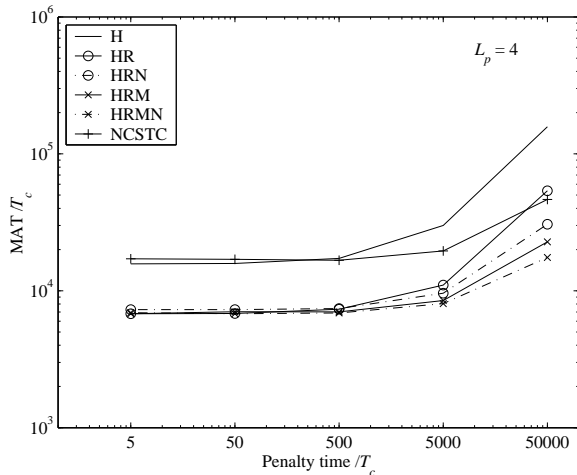
Due to the formidable analysis of the modified schemes in Subsections 2.3 and 2.4, we will use simulation to demonstrate their performance in Section 4.

4. NUMERICAL AND SIMULATION RESULTS

First we show examples on computing P_d and P_{fa} from (66) and (67) using numerical computation. To reduce the computation to a manageable level, we present results with $M = 2$, $L_p = 4$, SNR = -5 dB, $n_1 = 50$, $n_2 = 40$, $\Gamma_1 = 0.7$, $f_d = 10$ Hz, and

Table 1: The best setting values of $n_1, n_2, n_3, n_4, \Gamma_1, \Gamma_2, \Gamma_3, \Gamma_4$ and Γ_f for each scheme.

Scheme	n_1	Γ_1	n_2	Γ_2	n_3	Γ_3	n_4	Γ_4	Γ_f
H	220	5.43×10^4	-	-	-	-	-	-	-
HR	72	2.42×10^4	56	1.08×10^5	-	-	-	-	-
HRN	72	2.42×10^4	56	1.08×10^5	-	-	-	-	2.16×10^4
HRM	32	6.20×10^3	32	2.12×10^4	32	4.40×10^4	32	7.28×10^4	-
HRMN	32	6.20×10^3	32	2.12×10^4	32	4.40×10^4	32	7.28×10^4	2.16×10^4
NCSTC	128	6.50×10^4	-	-	-	-	-	-	-

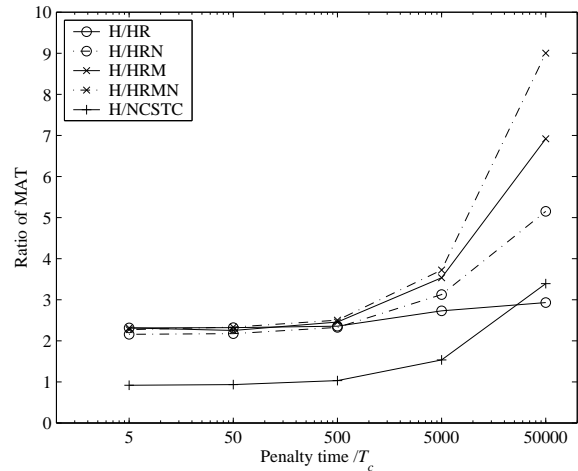

Fig.15: MAT of the conventional hybrid scheme and the proposed schemes versus penalty time.

$T_c = 10^{-6}$ s, while varying Γ_2 . Note that the pdf is normalized by σ_{1,H_1}^2 . The results are shown in Figs. 12 and 13.

The results in Figs. 12 and 13 are used to compute the MAT by using (39) at $P_d = 0.45$ and $P_{fa} = 0.02$, and the result is shown in Fig. 14. In the same figure, we also present the results from simulation for comparison purpose. We can see that analytical and simulation results agree reasonably well.

For performance comparison, we evaluate the MAT of the conventional hybrid scheme (H) and the proposed double-dwell hybrid-RAKE scheme (HR) with the same number of branches. We set the number of branches to $M = 4$ and the number of paths $L_p = 4$. For the conventional hybrid scheme, the phase of the PN signal fed to each correlator branch is delayed by $NT_c/4$ relative to the previous correlation branch (see Fig. 1). It means that 4 different phases are checked at a time. The maximum among them is compared with a threshold. If it exceeds the threshold, the tracking circuit is initiated. On the other hand, if it is lower than the threshold, the phase of the local PN signal is updated by T_c . According to this scheme, acquisition means identifying correctly the signal path having its phase aligned with the local PN phase.

We also simulate the performances of the pro-


Fig.16: Ratio of the MAT of the conventional hybrid scheme to the proposed schemes versus penalty time.

posed double-dwell hybrid-RAKE scheme with noise-only detection (HRN) described in Subsection 2.3 and the proposed hybrid-RAKE scheme with multiple-dwell (HRM) described in Subsection 2.4 and the proposed hybrid-RAKE scheme with both noise-only detection and multiple-dwell test (HRMN). We use 4 dwells for the HRM and HRMN schemes. In addition, the nonconsecutive search and joint triple-cell detection (NCSTC) proposed by [14] is also simulated under the same condition.

The PN sequence in the simulation is an m-sequence with polynomial $1 + x^4 + x^9$, so that the period is 511 chips and SNR = -5 dB. To obtain a fair comparison, we choose the integration length and threshold that give the minimum MAT in each scheme, by varying the integration length and threshold until a minimum is found for the penalty time of $5000T_c$. The minimum MAT occurs at parameter values shown in Table 1.

The first simulation results using the values in Table 1 are shown in Fig. 15, which plots the MAT (normalized by the chip duration T_c) versus the penalty time (also normalized by the chip duration). We can see that all the proposed schemes outperform the conventional hybrid scheme and the NCSTC scheme at any value of penalty time. As expected, the fastest proposed scheme is the proposed scheme with noise-

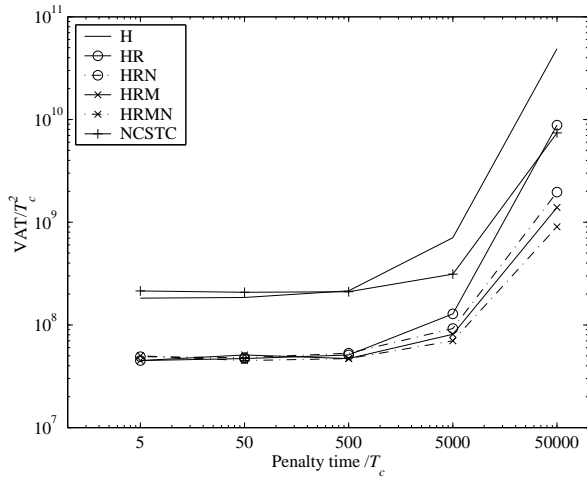


Fig.17: VAT of the conventional hybrid scheme and the proposed schemes versus penalty time.

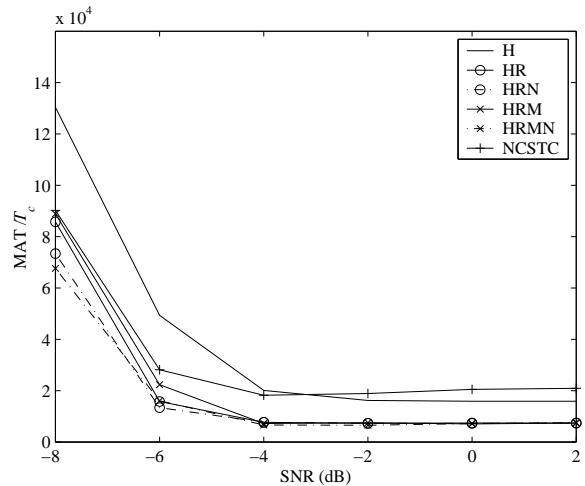


Fig.19: MAT of the conventional hybrid scheme and the proposed schemes versus SNR.

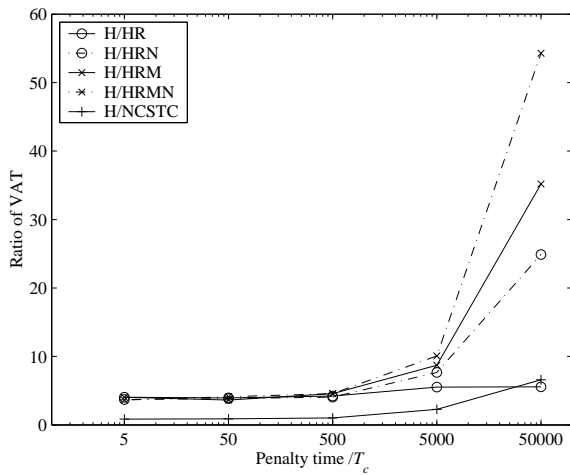


Fig.18: Ratio of the VAT of the conventional hybrid scheme to the proposed schemes versus penalty time.

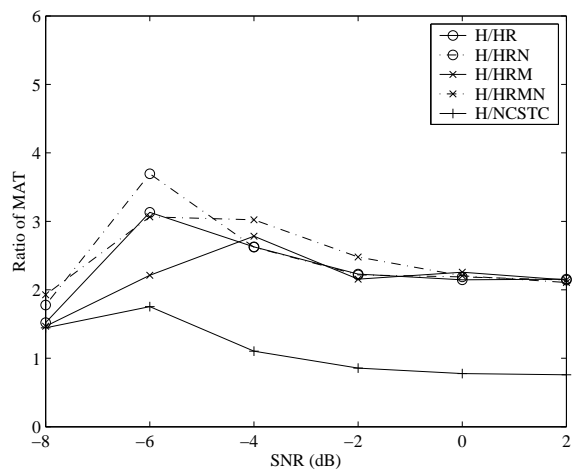


Fig.20: Ratio of the MAT of the conventional hybrid scheme to the proposed schemes versus SNR.

only detection and multiple dwells. When the penalty time is short, all four of the proposed schemes have similar performance. Figure 16 shows the ratio of the MAT of the conventional hybrid scheme over the MAT of all the proposed schemes. We can see that the proposed schemes acquire the PN phase faster than the conventional hybrid scheme by about 2 - 9 times, depending on the penalty time. VAT are shown in Fig. 17 and their ratios are shown in Fig. 18. We can see that the variances of the proposed schemes are reduced, compared to the conventional hybrid scheme

The last simulation results show the effect of SNR. The setting parameters in Table 1 are used. The simulation is run by varying SNR and the results are shown in Figs. 19 and 20. Figure 19 depicts the MAT versus SNR.

We can see that when the SNR decreases the MAT increases, as expected. Figure 20 shows that all the proposed schemes perform better than the conven-

tional hybrid scheme at any SNR. At high SNR, all of the four proposed schemes have similar performance.

From all simulation results, we can see that HRMN scheme gives the best performance with the highest complexity. However at small penalty time or large SNR, all of the four proposed schemes have similar performance. Therefore, to select a suitable scheme for a system, the penalty time and SNR are key parameters.

5. CONCLUSION

We proposed PN acquisition schemes for frequency-selective Rayleigh fading channel using RAKE structure and multiple-dwell technique. The RAKE structure provides robustness against the effect of multipath fading in the channel, while the multiple-dwell technique provides an improved acquisition time. Performance is verified by simulations which show that the proposed scheme acquires the phase faster than the conventional hybrid scheme and a previous

scheme that also used the RAKE structure, all with a similar amount of hardware.

Among the proposed schemes, adding noise-only detection and/or using multiple dwell technique help improve the performance when the penalty time is large or the SNR is small. However, the computation complexity also increases.

6. ACKNOWLEDGMENT

This work was supported by a Royal Golden Jubilee Scholarship from Thailand Research Fund, Bangkok, Thailand.

References

- [1] B. Sklar, *Digital Communications; Fundamentals and Applications*, pp. 538-542, P T R Prentice Hall, 1988.
- [2] C.E. Cook, F.W. Ellersick, L.B. Milstein and D.L. Schilling, *Spread-Spectrum Communications*, IEEE PRESS, 1983.
- [3] M.K. Simon, J.K. Omura, R.A. Scholtz and B.K. Levitt, *Spread Spectrum Communications Handbook*, McGraw-Hill, 1985.
- [4] C.-C. Fan and Z. Tsai, "Serial and Parallel Search with Parallel I-Q Matched Filter for PN Acquisition in PCS," *IEICE Trans. Commun.*, vol. E79-B, no. 9 pp. 1278 - 1286, Sep. 1996.
- [5] T. Samanchuen and S. Tantaratana, "An Improved Closed-Loop Coherent Pseudo-Noise Acquisition Scheme Using an Auxiliary Sequence," *IEICE Trans. Commun.*, vol. E85-B, no. 3, pp. 594-604, Mar. 2002.
- [6] S. Kang and Y.-H. Lee, "Rapid Acquisition of PN Signals for DS/SS Systems Using a Phase Estimator," *IEEE J. Select. Areas Commun.*, vol. 19, no. 6, pp. 1128-1137, Jun. 2001.
- [7] E.A. Sourour and S.C. Gupta, "Direc-Sequence Spread-Spectrum Parallel Acquisition in a Fading Mobile Channel," *IEEE Trans. Commun.*, vol. 38, no. 7, pp 992-998, July 1990.
- [8] B. Kang, "Performance Evaluation of DS/CDMA Hybrid Acquisition in Multipath Rayleigh Fading Channel," *IEICE Trans. Cummun.*, vol. E80-B, no. 8, pp. 1255-1263, Aug. 1997.
- [9] A.J. Viterbi, *CDMA Principles of Spread Spectrum Communication*, Addison-Wesley, 1995.
- [10] H.-S. Oh, C.-H. Lim and D.-S. Han, "Adaptive Hybrid PN Code Acquisition with Antenna Diversity in DS-CDMA Systems," *IEICE Trans. Commun.*, vol. E85-B, no. 4, pp. 716-722 Apr. 2002.
- [11] B. Sklar, "Rayleigh Fading Channels in Mobile Digital Communication Systems Part I: Characterization," *IEEE Communication Magazine*, pp. 136-146, Sep. 1997.
- [12] B. Sklar, "Rayleigh Fading Channels in Mobile Digital Communication Systems Part II: Mitigation," *IEEE Communication Magazine*, pp. 148-155, Sep. 1997.
- [13] R.R. Rick and L.B. Milstein, "Optimal Decision Strategies for Acquisition of Spread-Spectrum Signals in Frequency-Selective Fading Channels," *IEEE Trans. Commun.*, vol. 46, no. 5, pp. 686-694, May 1998.
- [14] O.-S. Shin and K.B. Lee, "Utilization of Multipaths for Spread-Spectrum Code Acquisition in Frequency-Selective Rayleigh Fading Channels," *IEEE Trans. Commun.*, vol. 49, no. 4, pp. 734-743, Apr. 2001.
- [15] J.G. Proakis, *Digital Communications*, McGraw-Hill, Singapore, 1995.
- [16] L.W. Couch II, *Digital and Analog Communication Systems*, Prentice-Hall, Inc., America, 2001.
- [17] M.K. Simon and M.-S. Alouini, *Digital Communication over Fading Channels : A Unified Approach to Performance Analysis*, John Wiley & Sons, Inc., 2000.
- [18] S. Fukumoto, M. Sawahashi, and F. Adachi, "Matched Filter-Based Rake Combiner for Wideband DS-CDMA Mobile Radio," *IEICE Trans. Commun.*, vol. E81-B, No.7, pp. 1384-1391, Jul. 1998.
- [19] A. Polydoros and C.L. Weber, "A unified approach to serial search spread-spectrum code acquisition—Path I: General theory," *IEEE Trans. Commun.*, vol. COM-32, pp. 542-549, May 1984.
- [20] H. Moon, "Performance of Double Dwell Acquisition with Continuous Integration Dectector in a Rician Fading Channel," *Proc. of IEEE 5th International Symposium on Spread Spectrum Techniques and Applications*, vol. 1, pp.111 -115 Sep. 1998.



Taweesak Samanchuen received the B.E. degree from King Mongkut's University of Technology, Thonburi, Bangkok, Thailand, in 1997 and M.S. degree from Sirindhorn International Institute of Technology, Thammasat University, Thailand, in 2000. He is currently working toward the Ph.D. degree. His research interests include spread spectrum communications and code synchronization.



Sawasd Tantaratana received his B.E.E. degree from the University of Minnesota in 1971, M.S. degree from Stanford University in 1972, and Ph.D. degree from Princeton University in 1977, all in electrical engineering. Since 1997 he has been with Sirindhorn International Institute of Technology, Thammasat University, Thailand, where he is currently the Director and Professor of Electrical Engineering. Previously, he has taught at King Mongkut's Institute of Technology, Thonburi, Thailand; Auburn University, Alabama, USA; and the University of Massachusetts at Amherst, Massachusetts, USA. He has also worked at AT&T Bell Laboratories in Holmdel, New Jersey, and at the National Electronics and Computer Technology Center (NECTEC), Bangkok, Thailand. From 1980-1981 he was a visiting faculty member at the University of Illinois at Urbana-Champaign, Illinois. Dr. Tantaratana is a Member of Eta Kappa Nu, Sigma Xi, IEICE, and a Senior Member of the IEEE. He was an Associate Editor for the IEEE Transactions on Signal Processing from 1996-1997. His current research interests include signal processing, digital filter design and realization, spread-spectrum systems, and wireless communications.